Journal of Magnetic Resonance 195 (2008) 116–120

Contents lists available at ScienceDirect

Journal of Magnetic Resonance

journal homepage: www.elsevier.com/locate/jmr

Communication

Coherence selection in double CP MAS NMR spectroscopy

Jen-Hsien Yang [a], Fang-Chieh Chou [b], Der-Lii M. Tzou [a,c,*]

[a] Institute of Chemistry, Academia Sinica, 128, Yen-Chiu-Yuan Road, Sec. 2, Nankang, Taipei 11529, Taiwan, ROC
[b] Department of Chemistry, National Taiwan University, Taipei 106, Taiwan, ROC
[c] Department of Applied Chemistry, National Chia-Yi University, Chia-Yi, Taiwan, ROC

ARTICLE INFO

Article history:
Received 5 March 2008
Revised 15 August 2008
Available online 23 August 2008

Keywords:
Solid-state NMR
Spectral editing
Coherent transfer
Double cross-polarization
Magic-angle spinning

ABSTRACT

Applications of double cross-polarization (CP) magic-angle spinning (MAS) NMR spectroscopy, via $^{1}H/^{15}N$ and then $^{15}N/^{13}C$ coherence transfers, for ^{13}C coherence selection are demonstrated on a $^{15}N/^{13}C$-labeled *N*-acetyl-glucosamine (GlcNAc) compound. The $^{15}N/^{13}C$ coherence transfer is very sensitive to the settings of the experimental parameters. To resolve explicitly these parameter dependences, we have systematically monitored the $^{13}C\{^{15}N/^{1}H\}$ signal as a function of the *rf* field strength and the MAS frequency. The data reveal that the zero-quantum coherence transfer, with which the ^{13}C effective *rf* field is larger than that of the ^{15}N by the spinning frequency, would give better signal sensitivity. We demonstrate in one- and two-dimensional double CP experiments that spectral editing can be achieved by tailoring the experimental parameters, such as the *rf* field strengths and/or the MAS frequency.

1. Introduction

Double cross-polarization (CP) magic-angle spinning (MAS) solid-state NMR spectroscopy was first introduced by Schaefer et al. in 1979 [1]. Later, the original one-dimensional (1D) technique was extended to two-dimensional (2D), from which the correlation spectra on the basis of heteronuclear chemical shifts [2,3] and dipole–dipole coupling [4] could be obtained. The 2D pulse sequence of a $^{1}H/^{15}N/^{13}C$ double CP experiment is given in Fig. 1. In the $^{13}C/^{15}N$ chemical shift correlation, the ^{1}H coherence is transferred into ^{15}N during the first CP period. Then, the ^{15}N chemical shift is allowed to evolve, and the ^{15}N coherence is subsequently transferred to ^{13}C during the second CP period for observation. Using the double CP coherence transfer, only the ^{13}C signals of those carbons coupled to the ^{15}N-labeled nitrogen are observable. Although the $^{1}H/^{15}N$ CP follows the conventional Hartmann–Hahn matching condition, where the spin locking fields are lying on the *xy*-plane, the $^{15}N/^{13}C$ CP requires a critical matching condition for the effective spin locking fields. In fact, as illustrated in the subsequent sections, the $^{15}N/^{13}C$ polarization transfer is explicitly dependent on the experimental parameters such as the chemical shifts, *rf* field strengths, and the MAS frequency. Furthermore, we will demonstrate that the $^{1}H/^{15}N/^{13}C$ double CP experiment is capable of spectral editing via 1D or 2D spectroscopy.

It has been pointed out that the matching condition of $^{15}N/^{13}C$ CP is so stringent that a slight mismatch can result in a considerable reduction of the double CP intensity [5,6]. Several schemes have been developed to improve the CP transfer efficiency [7–11]. In an alternative approach, Baldus and coworkers made a good use of low *rf* field strengths in the range of 1–5 kHz, which are comparable with the frequency offsets of the resonances, for specific coherence selection. Their frequency-selective double CP experiment is called SPECIFIC CP [5]. In principle, two coherent transfer pathways are accessible, depending on the experimental settings. At low MAS frequencies ($\omega_R < 10$ kHz) and large *rf* fields, the coherent transfer is dominated by the zero-quantum (ZQ) coherence transfer. In contrast, at high MAS frequencies ($\omega_R > 10$ kHz) and/or small *rf* fields, the transfer could be carried out by double-quantum (DQ) coherence [12]. To achieve an effective coherence transfer, in either case, the experimental parameters have to match certain requirements. In the ZQ transfer, the difference in the effective *rf* fields of the *I*- (^{15}N-) and *S*- (^{13}C-) channels must be equal to a multiple of the MAS frequency: $(\omega_{1I}^2+\Omega_I^2)^{1/2}-(\omega_{1S}^2+\Omega_S^2)^{1/2}=n\omega_R$. On the other hand, in the DQ transfer, the sum of the effective *rf* fields of the *I*- and *S*-channels shall be equal to a multiple of the MAS frequency: $(\omega_{1I}^2+\Omega_I^2)^{1/2}+(\omega_{1S}^2+\Omega_S^2)^{1/2}=n\omega_R$, where ω_{1I} and ω_{1S} denote the *rf* field strengths of the *I*- and *S*-channels, respectively, Ω_I and Ω_S are the frequency offsets of the associated ^{15}N and ^{13}C chemical shifts, respectively, ω_R is the MAS frequency of the sample. In this study, we applied *rf* fields in the range of 10–40 kHz for the $^{13}C/^{15}N$ ZQ coherence transfer. The *N*-[1,2-$^{13}C_2$]acetyl-D-[1-^{13}C,^{15}N] glucosamine (GlcNAc) compound was used to determine the dependence of signal sensitivity of the $^{13}C/^{15}N$ coherence transfer on the experimental parameters. The ZQ matching

* Corresponding author. Address: Institute of Chemistry, Academia Sinica, 128, Yen-Chiu-Yuan Road, Sec. 2, Nankang, Taipei 11529, Taiwan, ROC. Fax: +886 2 2783 1237.
E-mail address: tzou@ccvax.sinica.edu.tw (D. M. Tzou).

1090-7807/$ - see front matter © 2008 Elsevier Inc. All rights reserved.
doi:10.1016/j.jmr.2008.08.006

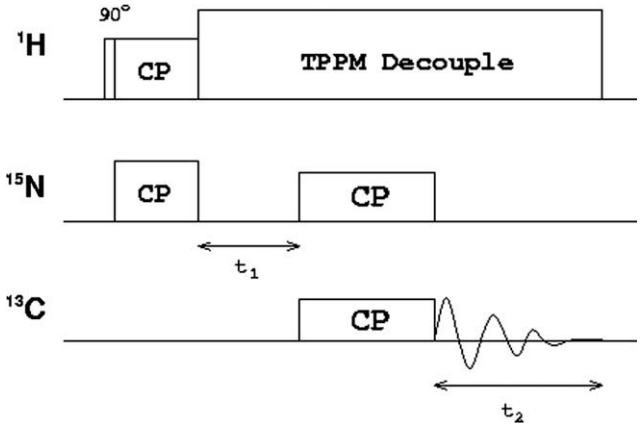

Fig. 1. Pulse sequence of double CP MAS NMR spectroscopy. The triple-resonance solid-state NMR experiment consists of two CP periods: $^1H/^{15}N$ and $^{15}N/^{13}C$ (I/S). The first CP is optimized to fulfil the Hartman–Hahn matching condition [17]. After the Hartman–Hahn matching, ^1H TPPM decoupling [18] is applied with a *rf* field strength of 79.3 kHz. The ^{15}N chemical shift, which is eliminated in the 1D version, evolves after the first CP in the t_1 dimension in the 2D experiment. All the double CP MAS NMR spectra were acquired with a Bruker (Spectrospin, Rheinstetten, Germany) Avance 300 MHz NMR spectrometer, equipped with a 4-mm triple resonance probe operating at ^1H, ^{13}C, and ^{15}N Larmor frequencies of 300.13, 75.47, and 30.3 MHz, respectively. Contact times of 1 and 5 ms were set for the double CPs. Powdered samples were packed in double-bearing 4 mm zirconium oxide MAS rotors. All experiments were carried out at ambient temperature and the sample spinning frequency was regulated within ±1 Hz by a spinning controller.

conditions corresponding to various Hartmann–Hahn matching conditions ($n = 0, n = \pm1, n = \pm2$) are resolved in a 2D spectrum array, in which the *rf* field strength and the MAS frequency are systematically varied. Typically, the coherence transfer carried out at $n = \pm1$ leads to a stronger signal intensity than that of $n = \pm2$. In our double CP experiment, spectral editing is achieved by tailoring either the *rf* field strength or the MAS frequency, as demonstrated in the 2D spectra measured for the powder samples of isotopically labeled GlcNAc and glycine. It is anticipated that it should be possible to combine such a coherence selection or spectral editing technique with other NMR schemes, such as REDOR spectroscopy [13], and, to extend it to specific 3D heteronuclear chemical shift correlation spectroscopy.

2. Theory

The Hamiltonian of an isolated I–S spin-pair in the doubly rotating frame is given by [14]

$$H = \omega_{1I}(t)I_y + \omega_{1S}(t)S_y + \Omega_I I_z + \Omega_S S_z + 2d_{IS}(t)I_z S_z, \tag{1}$$

where $\omega_{1I}(t) = -\gamma_I B_{1I}(t)$ and $\omega_{1S}(t) = -\gamma_S B_{1S}(t)$ for the I and S spins, respectively, Ω_I and Ω_S denote the time-independent resonance offsets. The dipolar term can be expanded into Fourier components:

$$d_{IS}(t) = \sum_{n=\pm1,\pm2} d_n \exp(-n\omega_R t)$$

and

$$d_{\pm1} = \mp\frac{d_{IS}}{2\sqrt{2}}\sin(2\theta)\exp(\pm i\varphi),$$

$$d_{\pm2} = \frac{d_{IS}}{4}\sin^2\theta\exp(\pm 2i\varphi),$$

$$d_{IS} = -\frac{\mu_0\gamma_I\gamma_S\hbar}{4\pi r_{IS}^3}. \tag{2}$$

Here, r_{IS} denotes the internuclear distance between the I and S spins, θ and φ the polar angles between the respective internuclear vector and the static magnetic field, γ_I and γ_S the gyromagnetic ratios of the I and S spins, respectively, and ω_R the MAS frequency. For simplicity, the contributions from the anisotropic chemical shielding are neglected in the Hamiltonian.

Following the treatment of Baldus et al. [5], the Hamiltonian H can be transformed to the tilted frame by the following transformation:

$$\tilde{H}^T = UH^TU^{-1}; \quad U = \exp[-i(\omega_{1I,\mathrm{eff}}I_z + \omega_{1S,\mathrm{eff}}S_z)t], \tag{3}$$

where

$$\omega_{1I,\mathrm{eff}}(t) = (\omega_{1I}(t)^2 + \Omega_I^2)^{1/2}$$

and

$$\omega_{1S,\mathrm{eff}}(t) = (\omega_{1S}(t)^2 + \Omega_S^2)^{1/2}.$$

In the new spin coordinate system where the new axes are tilted around the I_x and S_x axis lying along the effective field directions $I_{\mathrm{eff}}(t) = \omega_{1I}(t)I_y + \Omega_I I_z$ and $S_{\mathrm{eff}}(t) = \omega_{1S}(t)S_y + \Omega_S S_z$, respectively. For brevity, we retain only the flip-flop term in the subsequent treatment [5,7]:

$$H_{\mathrm{sec}} = \omega_{I,\mathrm{eff}}(t)I_z + \omega_{S,\mathrm{eff}}(t)S_z + d_{IS,\mathrm{eff}}(t)\times\left(\frac{I^+S^- + S^-I^+}{2}\right) + 2\varepsilon(t)I_zS_z, \tag{4}$$

where

$$d_{IS,\mathrm{eff}}(t) = d_{IS}(t)\sin\phi_I\sin\phi_S$$

and

$$\phi_I(t) = \sin^{-1}[\omega_{1I}(t)/\omega_{1I,\mathrm{eff}}(t)],$$

$$\phi_S(t) = \sin^{-1}[\omega_{1S}(t)/\omega_{1S,\mathrm{eff}}(t)],$$

$$\varepsilon(t) = d_{IS}(t)\cos\phi_I\cos\phi_S.$$

In the interaction frame transformed by the *rf* fields, the following time-independent ZQ Hamiltonian is obtained:

$$H_0 = d_{n,\mathrm{eff}}(I^+S^- + I^-S^+)/2, \tag{5}$$

where $d_{n,\mathrm{eff}} = d_n\sin\theta_I\sin\theta_S$, $n = \pm1, \pm2$;

$$\phi_I = \sin^{-1}\left[\omega_{1I}/\sqrt{\omega_{1I}^2 + \Omega_I^2}\right], \quad \phi_S = \sin^{-1}\left[\omega_{1S}/\sqrt{\omega_{1S}^2 + \Omega_S^2}\right]$$

when the $\omega_{I,\mathrm{eff}}(t) - \omega_{S,\mathrm{eff}}(t) = n\omega_r$ matching condition is satisfied. Since the Hamiltonian coefficients $d_{\pm1}$ is greater than $d_{\pm2}$, it is expected that the $n = \pm1$ sideband intensity is higher than the $n = \pm2$ sideband intensity. The corresponding DQ coherence transfer is also well documented in the literature [5,12].

3. Results

A specific $^{13}C/^{15}N$-isotope-labeled GlcNAc sample that exhibits four distinct resonances in the normal ^{13}C CP MAS spectrum was selected for the current study. As shown in Fig. 2, the ^{13}C CP MAS spectrum reveals a carbonyl carbon (^{13}CO) resonance at 175.5 ppm, two monosaccharide carbon residues ($^{13}C1$) with respect to the anomeric α- and β-forms at 93.0 and 96.8 ppm, respectively, and methyl carbon ($^{13}CH_3$) at 24.1 ppm. Unlike the $^1H/^{13}C$ or $^1H/^{15}N$ coherence transfer that fulfils the conventional Hartmann–Hahn condition, the double CP intensity arising from the $^1H/^{15}N/^{13}C$ coherence transfer pathway is rather sensitive to the experimental parameters, including the MAS, *rf* field and the carrier frequency. To resolve the parameter dependences more clearly, we have monitored the double CP intensity by varying the *rf* field strength and the MAS frequency systematically. Fig. 3

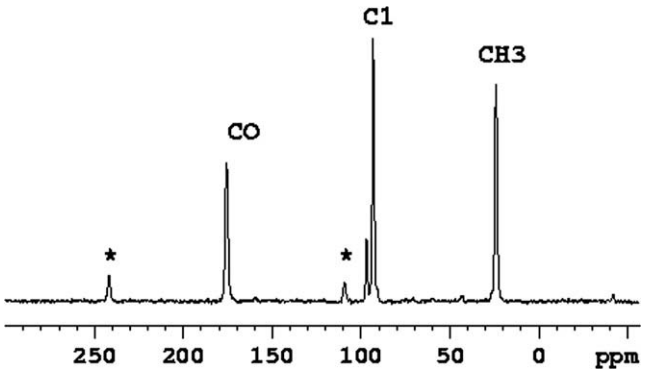

Fig. 2. Normal 1D $^{1}H/^{13}C$ CP MAS spectrum of amino monosaccharide *N*-[1,2-$^{13}C_2$]acetyl-D-[1-^{13}C;^{15}N] glucosamine (GlcNAc) specifically labeled with ^{13}C (99%) and ^{15}N (98%), which was purchased from Omicron, Biochemicals, Inc. (South Bend, IN). The sample was used without further processing. The *rf* field strength in the ^{1}H and ^{13}C channels was set to 50 kHz for CP, with a contact time of 1 ms. The experiment was carried out at an MAS frequency of 5000 Hz, with total transient number of 4096 and recycle delay of 5 s. The asterisks denote the sample spinning sidebands.

shows the $^{13}CO\{^{15}N\}$ intensity as a function of the *rf* field strength and MAS frequency. Consistent with previous reports [5,6], the $^{13}C\{^{15}N\}$ intensity is explicitly dependent on the *rf* field strength in the horizontal axis and the MAS frequency in the vertical axis, such that the $^{15}N/^{13}C$ CP transfers effectively only at certain combinations of the two. In fact, the matching condition is so critical that any modification of the variables may result in a substantial reduction in the resulting intensity. The sensitivities of these parameter settings are determined from the present and previous studies [6] to be around 200 Hz for the *rf* field strength and 500 Hz for the MAS and carrier frequencies. Apart from the sensitivities, the profile presents two different coherence transfers corresponding to MAS-dependent and MAS-independent pathways, which are labeled by vertical and tilted lines, respectively, in Fig. 3. The MAS-independent coherence transfer is assigned to the $n = 0$ matching condition, which is due to the higher order effects [12]. The MAS-dependent coherence transfer, which corresponds to the ZQ Hamiltonian discussed above, are assigned to $n = \pm 1$ and ± 2 sidebands. As expected, the two matching sidebands differ from each other by the MAS frequency approximately. Such a symmetrical double-maximum distribution pattern that denotes the $n = \pm 1$ and ± 2 ZQ coherence transfers resembles the double CP sensitivity measurement with respect to the carrier frequency reported previously [6]. In general, the MAS-dependent coherence gives arise to a much greater intensity, with typically at least a fivefold difference in magnitude, than the MAS-independent one. It is interesting to find that the ZQ coherence transfer corresponding to the $n = +1$ condition, in which the ^{13}C spin locking field is larger than that of the ^{15}N by the spinning frequency, would give better signal sensitivity than the $n = -1$ condition. Thus, it is better to fulfil the MAS-dependent matching condition, in particular for $n = +1$, for optimizing the double CP intensity, and for the application of coherence selection described below. Note that the overall intensity of the slice corresponding to MAS at 7000 Hz is some-

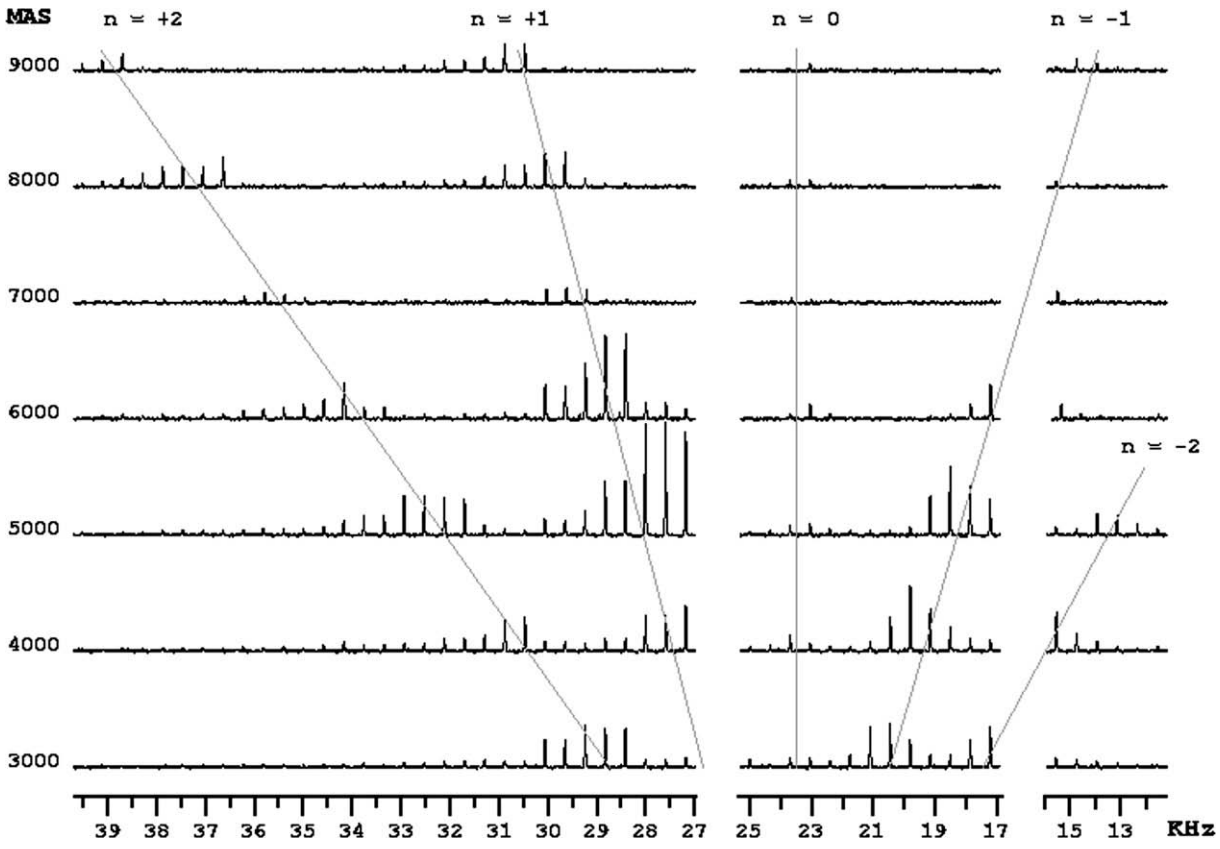

Fig. 3. Double CP sensitivity measurements of amino monosaccharide GlcNAc with multiple ^{13}C and ^{15}N isotope labeling. The ^{15}N-correlated^{13}C intensity of carbonyl carbon is monitored as a function of two variables: the *rf* field strength (^{13}C channel) and the MAS frequency. The *rf* field strength varies in the range 12–40 kHz with increments of 400 Hz and the MAS frequency from 3000 to 9000 Hz with increments of 1000 Hz. The sensitivity measurements are displayed in a 2D manner in which the *rf* field strength (^{13}C channel) and the MAS frequency in units of Hz are specified in the *x*- and *y*-axis, respectively. The *rf* field strength in ^{15}N (*I*-spin) was set to 26.3 kHz. In order to calibrate the linear scale of the *rf* field strength, we checked systematically the different power levels of the Bruker linear power amplifier (BLAX-1000) using a glycine powdered sample with natural abundance of isotopes. For clarity, those nonlinear portions are removed.

what less than for the adjacent slices. It is believed that this reduction is due to rotational resonance [15,16] when the MAS frequency reaches the difference in chemical shifts of the ^{13}C resonances of interest. This interpretation is further confirmed by the measurement on the [1-^{13}C,^{15}N]-glycine.

Apart from the ^{13}CO signal, we also monitored the methyl carbon $^{13}CH_3$ signal by double CP spectroscopy. The overall pattern as a function of the two variables the *rf* field strength and MAS frequency remained basically identical, but the overall intensity dropped significantly (see Fig. 1S and 2S in supplementary information). Compared to the ^{13}CO intensity, the double CP $^{13}CH_3$ intensity dropped at least tenfold in magnitude, indicating that the intensity can be attenuated by the ^{13}C chemical shifts or resonance offsets. Here, we propose that double CP MAS spectroscopy can specifically select the ^{13}C coherence by simply tailoring the experimental parameters and present only the $n = 1$ coherence transfer in the following analysis. A coherence selection of the $^{13}C\{^{15}N\}$ resonances with respect to the ^{13}CO, $^{13}C1$, and $^{13}CH_3$ of GlcNAc by setting the *rf* field strength of the ^{13}C channel to 38.3, 35.9, and 29.0 kHz, respectively, is shown in Fig. 4. Note that this spectral editing is achieved at the expense of the double CP signal intensity. In addition, as demonstrated in Fig. 4d–f, a similar coherence selection of the ^{13}CO, $^{13}C1$, and $^{13}CH_3$ resonances is achievable by setting the MAS frequencies to 6.0, 4.0, and 5.0 kHz, respectively. In comparison, the selectivity of the $^{13}C1$ and $^{13}CH_3$ coherences is better than that of the ^{13}CO, in which the ^{13}CO spectra (see Fig. 4a and d) are 'contaminated' by the residual $^{13}CH_3$ signal. By varying all the experimental parameters including carrier frequency, MAS frequency, and *rf* field strength, the quality can be further improved; the unwanted signal is limited within 5% of overall intensity (see Fig. 3S in supplementary information).

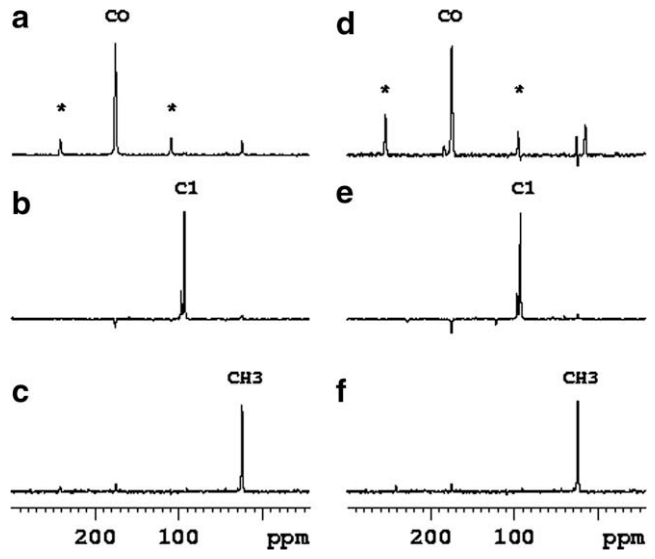

Fig. 4. Spectral editing of the ^{15}N-correlated ^{13}C spectrum of isotope-labeled GlcNAc compound by 1D double CP MAS spectroscopy. A coherence selection of (a) carbonyl carbon; ^{13}CO (175.5 ppm), (b) anomeric carbons; $^{13}C1$ (93.0 and 96.8 ppm), (c) methyl carbon; $^{13}CH_3$ (24.1 ppm) is achieved by setting the *rf* field strength (^{13}C channel) to 38.3, 35.9, and 29.0 kHz, respectively. The *rf* field strength in the ^{15}N channel was set to 6.5 kHz and the MAS frequency to 5 kHz. Independently, a coherence selection of (d) ^{13}CO (175.5 ppm), (e) $^{13}C1$ (93.0 and 96.8 ppm), (f) $^{13}CH_3$ (24.1 ppm), the same as (c), is also obtained by experimentally setting the MAS frequency to 6.0, 4.0, and 5.0 kHz, respectively. The *rf* field strengths in the ^{13}C and ^{15}N channels were set to 11.7 and 6.5 kHz. The double CP ^{13}C intensity was normalized to equal height for comparison. The doublet pattern observed from the C1 residue is due to the anomeric α- and β-forms. The asterisks denote the sample spinning sidebands. For each 1D spectrum, 1024 scans were acquired and recycle times of 5 s were used for all experiments.

2D coherence selection for $^{1}H/^{15}N/^{13}C$ triple resonance systems has been demonstrated with the $^{15}N/^{13}C$-labeled GlcNAc and glycine. As shown in Fig. 2, GlcNAc revealed distinct amide-^{15}N correlated ^{13}C resonances widely distributed in ^{13}C chemical shift, and glycine exhibited two amine-^{15}N coupled ^{13}C residues, namely $^{13}C_\alpha$ and ^{13}CO. In the ^{15}N (ω_1) dimension, the amide and amine resonances differ by approximately 80 ppm. By a judicious choice of the MAS frequency and the *rf* field strength, coherence selections of the ^{13}CO signal on GlcNAc and the $^{13}C_\alpha$ on glycine were demonstrated by 2D double CP MAS spectroscopy. Instead of mixing the two isotope-labeled compounds, we conducted the 2D double CP experiment under the same experimental conditions on the two samples separately. The two sets of double CP spectra were superimposed as shown in Fig. 5a and b, in which the coherence selections of the ^{13}CO resonances of GlcNAc (Fig. 5b) and the $^{13}C_\alpha$ residue from glycine (Fig. 5a) are indicated. We demonstrate that

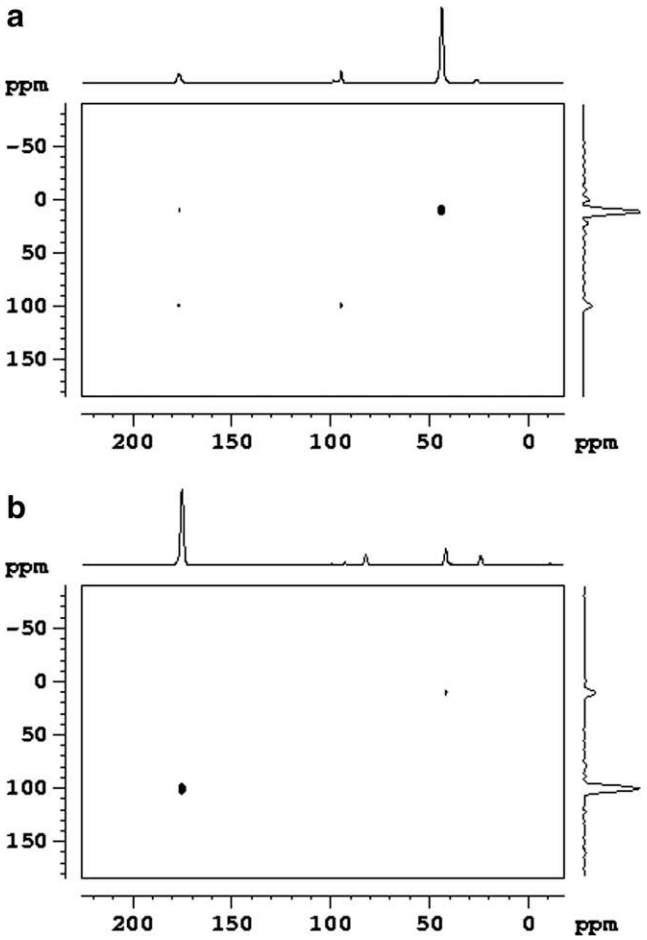

Fig. 5. 2D coherence selection double CP NMR spectroscopy on two isotope-labeled compounds: ^{13}C (99%) and ^{15}N (98%) double-labeled [1,2-^{13}C;^{15}N]glycine purchased from Isotech Inc. (Miamisburg, OH) and the isotope-labeled GlcNAc described in Fig. 2. 2D double CP NMR spectra were acquired on each of these two samples with the following experimental settings: (a) *rf* field strengths for ^{13}C and ^{15}N of 20.4 and 32.3 kHz and MAS of 6000 Hz; (b) *rf* field strengths for ^{13}C and ^{15}N of 28.5 and 24.0 kHz and MAS of 7000 Hz. Individual 2D spectra were then superimposed without modification to represent the coherence selections of ^{13}CO and $^{13}CH_2$ resonances originating from the samples, respectively. Less than 5% of the maximal intensity was set as a threshold for noise in the 2D contour plot. Projections along the ^{15}N resonance frequency (ω_2) and the ^{13}C resonance frequency (ω_1) axes are displayed. Total of 2048 complex points were collected in t_2 and either 256 complex points were in t_1 dimension. A recycle delay of 5 s was used in the 2D experiment and 32 scans were acquired for each t_1 increment. The ^{15}N chemical shift was externally referenced to ^{15}N isotope-labeled ammonia chloride at 16.07 ppm.

both 1D and 2D double CP MAS spectroscopy are capable of specifically selecting coherences of the ^{15}N-correlated ^{13}C resonances by simply tailoring the experimental parameters.

4. Conclusions

By making use of the stringent matching condition of the ZQ coherence transfer, we have shown that double CP MAS spectroscopy can be used to select specific coherences by tailoring one of the experimental settings, such as the *rf* field strength or the MAS frequency. In either case, a coherence selection of ^{15}N-correlated ^{13}C residues in isotope-labeled GlcNAc is feasible. We have demonstrated that double CP MAS solid-state NMR spectroscopy serves as a reliable and sensitive tool for the spectral editing of ^{13}C signals. In this work, we have examined the signal sensitivity of double CP MAS spectroscopy systematically. This 2D spectrum array displays a general matching criterion on which the settings of double CP experiments are critically relying.

Acknowledgments

We thank Jerry C.C. Chan (National Taiwan University) for helpful discussion and Wan-Sheung Li for the assistances in preparing the manuscript. This research was supported by Grant NSC 96-2113-M-001-011 from National Science Council of Taiwan.

Appendix A. Supplementary data

Supplementary data associated with this article can be found, in the online version, at doi:10.1016/j.jmr.2008.08.006.

References

[1] J. Schaefer, R.A. Mckay, E.O. Stejskal, Double-cross-polarization NMR of solids, J. Magn. Reson. 34 (1979) 443–447.
[2] T. Fujiwara, K. Sugase, M. Kainosho, A. Ono, A. Ono, H. Akutsu, C-13–C-13 and C-13–N-15 dipolar correlation NMR of uniformly labeled organic-solids for the complete assignment of their C-13 and N-15 signals—an application to adenosine, J. Am. Chem. Soc. 117 (1995) 11351–11352.
[3] E.R.H. Vaneck, W.S. Veeman, Solid-state 2D-heteronuclear Al-27–P-31 correlation NMR-spectroscopy of aluminophosphate Vpi-5, J. Am. Chem. Soc. 115 (1993) 1168–1169.
[4] K.V. Ramanathan, S.J. Opella, High-resolution solid-state C-13–N-14 and C-13–N-15 heteronuclear correlation spectroscopy, J. Magn. Reson. 86 (1990) 227–235.
[5] M. Baldus, A.T. Petkova, J. Herzfeld, R.G. Griffin, Cross polarization in the tilted frame: assignment and spectral simplification in heteronuclear spin systems, Mol. Phys. 95 (1998) 1197–1207.
[6] D.L.M. Tzou, A solid-state NMR application of the anoineric effect in carbohydrates: galactosamine, glucosamine, and *N*-acetyl-glucosamine, Solid State Nucl. Magn. Reson. 27 (2005) 209–214.
[7] M. Baldus, D.G. Geurts, S. Hediger, B.H. Meier, Efficient N-15–C-13 polarization transfer by adiabatic-passage Hartmann–Hahn cross polarization, J. Magn. Reson. A 118 (1996) 140–144.
[8] S. Hediger, B.H. Meier, N.D. Kurur, G. Bodenhausen, R.R. Ernst, NMR cross-polarization by adiabatic passage through the Hartmann–Hahn condition (Aphh), Chem. Phys. Lett. 223 (1994) 283–288.
[9] S. Hediger, B.H. Meier, R.R. Ernst, Adiabatic passage Hartmann–Hahn cross-polarization in NMR under magic-angle sample-spinning, Chem. Phys. Lett. 240 (1995) 449–456.
[10] S.M. Zhang, C.L. Czekaj, W.T. Ford, Enhancement of polarization transfer under high-speed MAS using a quasi-adiabatic cross-polarization sequence, J. Magn. Reson. A 111 (1994) 87–92.
[11] S.M. Zhang, Quasi-adiabatic polarization transfer in solid-state NMR, J. Magn. Reson. A 110 (1994) 73–76.
[12] B.H. Meier, Cross polarization under fast magic angle spinning—thermodynamical considerations, Chem. Phys. Lett. 188 (1992) 201–207.
[13] T. Gullion, J. Schaefer, Rotational-echo double-resonance NMR, J. Magn. Reson. 81 (1989) 196–200.
[14] M. Mehring, Principles of High Resolution NMR in Solids, second ed., Springer, Berlin, 1983.
[15] K. Takegoshi, K. Nomura, T. Terao, Selective homonuclear polarization transfer in the tilted rotating frame under magic angle spinning in solids, J. Magn. Reson. 127 (1997) 206–216.
[16] P.R. Costa, B.Q. Sun, R.G. Griffin, Rotational resonance tickling: accurate internuclear distance measurement in solids, J. Am. Chem. Soc. 119 (1997) 10821–10830.
[17] S.R. Hartmann, E.L. Hahn, Nuclear double resonance in the rotating frame, Phys. Rev. 128 (1962) 2043–2053.
[18] A.E. Bennett, C.M. Rienstra, M. Auger, K.V. Lakshmi, R.G. Griffin, Heteronuclear decoupling in rotating solids, J. Chem. Phys. 103 (1995) 6951–6954.